Satellitesimal formation in a circumplanetary disk and pebble accretion

*Yuhito Shibaike[1], Satoshi Okuzumi[1], Takanori Sasaki[2]

1.Department of Earth and Planetary Sciences, Tokyo Institute of Technology, 2.Department of Astronomy, Kyoto University

It has been recently suggested that planetesimals rapidly grow to the cores of gas giants by accreting a number of cm-sized solid particles called pebbles. We investigate how this pebble accretion mechanism affects satellite formation around gas giants. We construct a simple but comprehensive model that treats 1) the growth and radial transport of pebble-sized dust particles in a protoplanetary disk and in a circumplanetary disk around a gas giant, 2) the inflows of the gas and pebbles from protoplanetary to circumplanetary disks, and 3) pebble accretion by satellitesimals in a circumplanetary disk.
We found that most of pebbles flow into a circumplanetary disk not from the high-altitude of the disk but from the mid-plane against gas outflows. We also found that the growth processes of pebbles in a circumplanetary disk are divided into two much different ways; 1) satellitesimal formation by direct collisional growth of pebbles and subsequent satellite formation by direct collisional growth of the satellitesimals in a critical orbit, and 2) pebble accretion by large satellitesimals outside of the critical orbit. The critical orbit is moved by the conditions of the disk and pebbles. We introduce a parameter x, the ratio of the two mass fluxes of pebbles; flowing into the circumplanetary disk and drifted from the outer region of the protoplanetary disk. When x = 1, the critical orbit is in $r \sim 20\ R_J$ in the circumplanetary disk around a Jupiter-like planet with the mass of $0.4\ M_J$. However, when x = 0.1, the critical orbit is in $r \sim 3\ R_J$. Outside of the critical orbit, large satellitesimals accrete pebbles within their accretion radiuses. The radius expands dramatically when the mass of the satellitesimal reaches 10^{23}-10^{24} g, and the satellitesimal grows rapidly after that.
In conclusion, we paved the way for the formation of satellitesimals in a circumplanetary disk and reveal a rough picture of the pebble accretion by the satellitesimals.

Keywords: Satellite, Satellite formation, Pebble accretion , Circumplanetary disk, Satellitesimal, Gas planet

Accretion of icy pebbles by rocky planetary embryos in cooling protoplanetary disks

Takao Sato[1], *Satoshi Okuzumi[1], Shigeru Ida[2]

1.Department of Earth and Planetary Sciences, Tokyo Institute of Technology, 2.Earth-Life Science Institute, Tokyo Institute of Technology

Standard accretion disk models suggest that the snow line in the solar nebula migrated interior to the Earth's orbit in a late stage of nebula evolution. In this late stage, a significant amount of ice could have been delivered to 1 AU from the outer regions of the disk in the form of mm to dm-sized icy particles called "pebbles." This raises the question as to why the present Earth is so depleted of water.
In this study, we quantify the amount of icy pebbles accreted by terrestrial embryos in a cooling protoplanetary disk assuming that no mechanism halts the pebble flow outside the terrestrial planet forming region. We use a simplified version of the coagulation equation to calculate the formation and radial inward drift of icy pebbles in a protoplanetary disk. The pebble accretion cross section of an embryo is calculated using analytic expressions presented by recent studies. We find that the final mass and water content of terrestrial embryos strongly depends on the radial extent of the gas disk, the strength of disk turbulence, and the time at which the snow lines arrives at 1 AU. The disk's radial extent sets the lifetime of the pebble flow, while turbulence determines the density of pebbles at the midplane where the embryos reside. We find that the final water mass fraction of the embryos falls below that of the present Earth (0.023 wt%) only if the disk's radial extent is 100 AU or less, turbulence is strong at 1 AU, and the snow line arrives at 1 AU later than 2-4 Myr after disk formation. If the solar nebula extended to 300 AU, initially rocky embryos would have evolved into icy planets of 1-10 Earth masses unless the snow-line migration was slow. If the proto-Earth contained water of ~ 1 wt% as might be suggested by the density deficit of the Earth's outer core, it would have been possible for the proto-Earth to form with weaker turbulence and with earlier (> 0.5-2 Myr) snow-line migration.
Reference: Sato, T., Okuzumi, S., & Ida, S. 2016, A&A, in press (arXiv:1512.02414)
Figure: Time evolution of the mass and water fraction of an initially purely rocky embryo of the initial mass of 0.1 Earth mass placed at 1 AU in a cooling protoplanetary disk with the outermost radius of 100 AU. The curves show how the mass and water fraction evolve with time if the snow line reaches 1 AU at different times (0.5, 1, 2, 3, 4, and 5 Myr from left to right) after disk formation. The dashed and dotted lines mark the water fraction of 0.023 wt% (corresponding to the current terrestrial value estimated from the ocean mass) and 1 wt% (a theoretical upper limit on the primordial terrestrial value estimated from the mass deficit of the outer core), respectively. The left, center, and right panels are for turbulence parameters of 10^{-4}, 10^{-3}, 10^{-2}, respectively.

Keywords: snow line, terrestrial planets, water

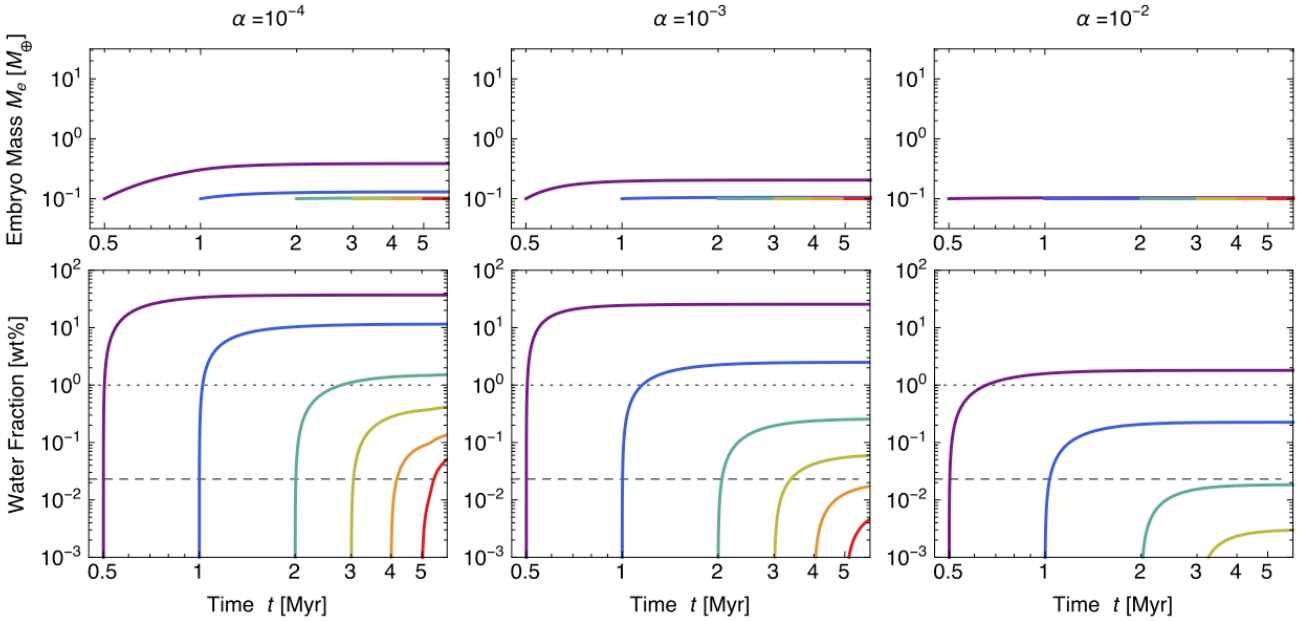

Numerical simulation of collisions between sintered icy dust aggregates

*Sin-iti Sirono[1], Haruta Ueno

1.Department of Earth and Planetary Sciences, Nagoya University

Collision of dust aggregates is a critical step in planetary formation. In the outer regions of a protoplanetary nebula, the main component of a dust grain is ice. Because ice is volatile material, it sublimes and recondenses in a protoplanetary nebula. Dust grains are connected by surface tension, leading to formation of a neck between grains. A neck has a concave surface, in contrast to the other parts of a grain having a convex surface. The equilibrium vapor pressure depends on the shape of surface. A concave surface has a lower vapor pressure than a convex surface. Because the gas pressure is uniform around a dust aggregate, ice molecules sublime from convex surface and recondense on concave surface. This process is called sintering. Sintering induces growth of a neck between grains. A grain can roll against the neighboring grain keeping a connection between grains. This rolling efficiently dissipate the kinetic energy and enables sticking in a collision. However, the rolling requires breakup of a grown neck after sintering. Therefore, it can be expected that sintering strongly affects collisional outcome of icy dust aggregates.
We performed 2-D collision simulations including the effects by sintering. A neck is approximated by an elastic cylinder. The degree of sintering corresponds to the radius of a neck. Head on collisions are simulated. Aggregates without sintering can stick if the collision velocity is less than 50 m/s. We investigated this critical velocity below which collisional growth is possible. When the colliding aggregate is produced by BCCA(Ballistic Cluster Cluster Aggregation) algorithm and sintering degree is high (neck radius/grain radius=0.7), the critical velocity decreases to around 20 m/s. If the degree of sintering is low (neck radius/grain radius=0.2), the necks are broken efficiently and reconnect through non-sintered necks. Then the difference in collisional outcomes is negligible.
When the packing fraction of an aggregate is high, the critical velocity is around 1 m/s. Above this velocity, collisional outcome is bouncing. This is because elasticity of an aggregate is high in this case. The induced stress is higher than the strength of contacting region on the aggregate surface, and the colliding aggregates bounce. When the collision velocity is higher than 20 m/s, Fracturing proceeds around the contacting region and fragments are produced. The amount of fragments is a few % when the collision velocity is 20 m/s.
From these results, sintering hinders collsional growth of icy dust aggregates. Aggregates infall to the central star due to gas drag. Within a sintering region, the infalling velocity differs from that in non-sintering region because the maximum aggregate size is limited by sintering. This velocity contrast produces a contrast in surface density in a protoplanetary nebula. The heterogeneity in solid component might affect planetary formation processes.

Keywords: sintering, dust aggregate, collision

From planetesimals to planets in turbulent protoplanetary disks

*Hiroshi Kobayashi[1], Hidekazu Tanaka[2], Satoshi Okuzumi[3]

1.Department of Physics, Nagoya University, 2.Tohoku University, 3.Tokyo Institute of Technology

In turbulent protoplanetary disks, planetesimals are stirred by turbulence, resulting in orderly growth. As planetesiamls grow via collisions, the escape velocities of planetesimals increase and therefore gravitational forcusing becomes important, which ignites runaway growth. The onset of runaway growth modifies the size distribution of planetesimals; the total mass of planetesimals is in the size of planetesimals at the onset of runaway growth. The planetesimal size determines the final mass of planets and the formation timescale. We deribe the size of planetesimals at the onset of runaway growth as a function of the turbulence strength, the surface density of the disk and distance from the host star. Using the result, we discuss constraints on the solar system formation.

Keywords: planet formation, planetesimal, turbulence

Local numerical simulations of axisymmetric two-dimentional instabilities in the dust layer of a protoplanetary disk

*Isamu Onishi[1], Minoru Sekiya[1]

1.Department of Earth and Planetary Sciences, Kyushu University

Two different processes have been proposed for the formation of planetesimals: mutual sticking of dust aggregates, and the gravitational instability of the dust layer. The critical density of the gravitational instability is hundreds times the gas density. However, the turbulent diffusion may prevent dust particles to settle toward the midplane of the protoplanetary disk, and the condition for the gravitational instability is difficult to be satisfied.

The streaming instability by Youdin & Goodman (2005) concentrates dust particles and boosts the planetesimal formation. The streaming instability is very efficient to form dust clumps in the case where dust particles have the stopping time on the order of the Keplerian orbital period (meter-sized particles). However, the streaming instability grows very slowly for small dust particles (1mm or less).

In this work, we carried out numerical simulations of motions of dust particles and gas in the dust layer of a protoplanetary disk. We assume the axisymmetry with respect to the rotation axis of the protoplanetary disk. We employ the local shearing-box approximation. We take account of the radial tidal force as well as the vertical force due to the stellar gravity, the gas drag force acting on dust particles and its back reaction. We include the effect of global pressure gradient by adding radial force to dust particles. We omit the effects of magnetic fields and the self-gravity.

We use the Athena code developed by Bai & Stone (2010) for numerical simulations. We report the results over a wide range of parameters, and consider comprehensively the causes of the instabilities in the dust layer of a protoplanetary disk.

Keywords: protoplanetary disk, dust, instability, planetesimal

New Condition for The Rossby Wave Instability

*Tomohiro Ono[1], Takayuki Muto[2], Taku Takeuchi, Hideko Nomura[3]

1.Department of Astronomy, Kyoto University, 2.Division of Liberal Arts, Kogakuin University, 3.Department of Earth and Planetary Sciences, Tokyo Institute of Technology

Recent observations have revealed the protoplanetary disks having non-axisymmetric structures, but the origin is still unknown. The Rossby wave instability (RWI) is one of the candidates of the origin. The RWI is a hydrodynamic instability in differential rotation disks, which forms non-axisymmetric large-scale vortices when disk profiles have a rapid radial variation. Previous works propose each of the necessary condition and the sufficient condition for the RWI. However, we are ignorant of the *necessary and sufficient* condition for the RWI.
In this work, we perform linear stability analyses of the RWI for barotropic flow on a wide parameter space. We calculate parameters for marginally stable states to the RWI. We find that the co-rotation radius is located at the background vortensity minimum with large concavity if the RWI is marginally stable. This allows us to check the stability against the RWI easily. We newly derive the *necessary and sufficient* condition for the RWI in semi-analytic form. It is expected that the new condition is available except when the width of the radial variation is much less than the scale height of the disks. The new condition and method will be useful for interpretations of observations and non-linear numerical simulations.

Keywords: protoplanetary disk, hydrodynamic instability, linear stability analysis

Planetesimal Impact Simulations by Godunov SPH Method for Elastic Dynamics with the Effects of Rocks

*Keisuke Sugiura[1], Shu-ichiro Inutsuka[1], Hiroshi Kobayashi[1]

1.NAGOYA UNIVERSITY Graduate School of Science

The earth and other rocky planets are supposed to be formed via collisional coalescences of planetesimals in protoplanetary disks. To understand the origins of rocky planets and characteristic shapes of asteroids we have to study the detail of outcomes of collisions between planetesimals. Laboratory experiments for disruptive collisions have been conducted, but they cannot treat objects larger than several ten centimeters or the velocity higher than several kilometers per second. Hence numerical simulation is powerful and effective method to study planetary collisions.

Many previous works on simulation of planetary collisions have used Smoothed Particle Hydrodynamics (SPH) method, which is one of the computational fluid dynamics methods using Lagrangian particles. However the most popular form of SPH method (the standard SPH method) has several problems. In particular, its spatial accuracy is lower than first order in disordered particle distribution; it utilizes artificial viscosity that tends to cause particle penetration in strong shock waves; the tensile instability, which is numerical instability, occurs in tension-dominated region. Moreover the effects of solids such as deviatoric stress are generally ignored in protoplanet collisions mostly in cases where self-gravity is dominant. The influence of the effects of solids for large protoplanet impacts is not fully discussed. Thus we should consider those effects, which requires us to develop an appropriate numerical simulation method.

Godunov SPH method (Inutsuka 2002) is proposed to solve the problems in the standard SPH method. The Godunov SPH method achieves second-order accuracy in space. To avoid the use of artificial viscosity it uses Riemann solver, which can introduce (possibly) minimum but sufficient physical viscosity. Moreover the Godunov SPH method can solve the tensile instability by selecting appropriate order of interpolation that is used in the equation of motion (Sugiura and Inutsuka 2016). We further extend the Godunov SPH method to elastic dynamics, and implement several models represent the effects of realistic solid material such as fracture. In this talk, we show the results of numerical simulations for planetesimal collisions that account for the effects of solid material, and discuss its influence.

Keywords: Planetesimals, collisional destruction, numerical simulation, elastic dynamics , Godunov SPH method

Scaling of impact-generated cavity-size for highly porous targets and its application to cometary surfaces

*Takaya Okamoto[1], Akiko Nakamura[2]

1.Planetary Exploration Research Center, Chiba Institute of Technology, 2.Department of Planetology, Graduate School of Science, Kobe University

Recent spacecraft missions have brought us the information of highly porous small bodies. The detail images of these bodies show variety of the surface. One of the interesting findings is that the depressions on comets look shallower than the simple craters such as on the moon, that is the depth-to-diameter ratio of the depressions are smaller than ~0.2. Although the mechanisms for the formation of the depressions such as collapse after the sublimation of the sub-surface volatile (Vincent et al., 2015) and activities after impact such as sublimation and viscous relaxation (e.g. Cheng and Dombard 2006, Thomas et al., 2013) are controversial, the shape of the cavity formed on highly-porous surface by impact itself is not understood well.
We performed impact experiments of sintered glass-bead targets with porosity of ~94%, and 87%, as well as gypsum targets with porosities of ~50% and pumice targets with those of 74%. The cavity created by the impact has maximum diameter at some depth from the target surface. The shape of the cavity is called bulb-shape cavity (Okamoto et al., 2013).The maximum diameter, D_{max} and the bulb depth, d_b of the cavity were analyzed. In addition to the results of this study, we also compiled the results of previous impact experiments for crater sizes in which the targets with porosity larger than 30% were used. Then new empirical scaling relations for the wide range of target porosity were obtained.
We applied the relations to comets. The surface strength and the particle size of the comet Tempel 1 are estimated to be of the orders of 10^1–10^3 Pa, and larger than ~50 μm, respectively. The ratio of bulb depth to the maximum diameter is also calculated from the scaling relations. The results show that the ratio on the weak surface with the strength less than 100 Pa was smaller than the depth-to-diameter ratio of simple craters, ~0.2. It suggests that shallow depressions on comets could be formed only by impact without subsequent activities, such as sublimation and viscous relaxation.

Keywords: porosity, hypervelocity impact experiment, comets

Cratering on iron alloy: Temperature and impact velocity effe cts

*Ryo Ogawa[1], Akiko Nakamura[1], Ayako Suzuki[2], Sunao Hasegawa[2]

1.Graduate School of Science, Kobe University, 2.Institute of Space and Astronautical Science

Introduction: Planetary differentiation could occur on planetesimals with diameters more than 20 km to form iron cores (Moskovitz and Gaidos, 2011). It is noted that the core formation occurred 0.3-0.6 million years after the most primitive material "CAI" was formed (Kruijer et al., 2014). That is, the core formation is a very primitive event and important to understand the early stage of the planetary evolution.
Currently, much attention is paid to an M-type asteroid 16 Psyche. Psyche may be the exposed iron core of a protoplanet and the Psyche orbiter mission is one of five Discovery Program semifinalist proposals. In order to get better understanding of planetary formation and evolution through such space mission, we have to understand about impact process on the surface of iron bodies. We performed impact experiments and simulations and examined the effects of temperature, impact velocity, on a cratering on iron material to collect basic data and examine model parameters (Ogawa et al., Shototsu Kenkyukai (in Japanese) 2016). In this study, we performed impact experiments and simulations with copper projectile which has well-defined material parameters to examine the effect of the projectile material. Furthermore, we performed numerical simulations of planetary scale cratering and compared them with the laboratory-scale ones.
Experimental method: We performed impact experiments with velocities of 6.8-7.3 km/s under 0.5-5.0 Pa using a two-stage light-gas gun at the Institute of Space and Astronautical Science (ISAS). Our targets were iron alloy (SS400) cubes with 50 mm each side. Projectiles were copper spheres of 3.2 mm in diameter. We used room-temperature (298 K) and low temperature (150 K) targets. The target material has brittle-ductile transition temperature at about 200 K. We simulated the cratering on the iron alloy using a shock physics code "iSALE" under the same conditions as the experiments. We used the Johnson-Cook strength model parameters of oxygen-free copper (Johnson and Cook, 1983) for projectiles and SS400 which we determined in our previous study for the targets. Moreover, we simulated planetary scale impacts with the stainless steel impactors of 0.02-5 km in diameter and SS400 targets of 0.2-200 km in diameter and examined the effect of the size using PI scaling.
Results of experiments: The craters of the low-temperature targets were shallower than the room-temperature targets at low impact velocity (2 km/s). However, the effect of temperature on depth couldn't be seen at high velocity (4-6.5 km/s). Moreover, we also couldn't find the effect of the temperature on diameter. Some of the iron alloy's strength increases by cooling (e.g. Petrovic, 2001). Therefore, the craters on the room-temperature targets were deeper than the low-temperature targets. On the other hand, the adhesion of the projectiles on the craters were seen in the experiments and simulations. In order to explain why the effect of temperature on depth wasn't seen at high impact velocity, we have to examine other effects than the strength-increase by cooling.
Results of simulations: The effect of temperature on the crater depth was less than those of the experiments. We haven't found why but it might be because the copper's Johnson-Cook parameters were 1/3-1/5 of those of SS400. A comparison between the simulation and laboratory results using PI scaling shows that craters were deeper in planetary scale than laboratory-scale at low impact velocity. Moreover, the craters on the low-temperature targets were as deep as room-temperature targets in planetary scale.

Keywords: Iron, Crater, Impact

Experimental estimate of mass loss rate by cratering for rubble-pile asteroids

*ERI TATSUMI[1], Seiji Sugita[1]

1.The University of Tokyo

Both Ground-based and spacecraft observations suggest that many small asteroids (< 10 km) have rubble-pile structures based on spin-rate, density, and geological features [1]. Recently theoretical study indicated that cratering might play a decisive role for size-frequency distribution of the main-belt asteroids besides catastrophic disruption [2]. Cratering on rubble-pile targets, which are loosely combined by small gravities and/or cohesions, has not been fully understood, although there are a few sets of experiments [3]. In this study, we conducted impact experiments to construct new scaling law for coarse-grained targets simulating the rubble-pile asteroid surfaces.
Impact experiments: We used two vertical guns in the Univ. of Tokyo and ISAS, for impact velocities 79 - 224 m/s and 1 - 6 km/s, respectively. We used polycarbonate projectiles 0.76 - 0.77 g for the former gun and 0.068 g for the latter gun. Pumice blocks (~7, 9, and 16 mm), basalt blocks (~ 10, and 18 mm) are used as boulder target simulants. The cross-section profiles were obtained by a laser profiler (Keyence, LJ-V). In order to observe the cross-section during cratering, we also conducted quarter-space experiments and recorded by a high-speed camera (NAC, Q1v).
Results and analyses: If target grain sizes do not influence cratering, crater sizes are the same sizes on sand targets. However, our results suggested that although high-velocity impacts (>4 km/s) formed similar crater sizes as sand targets, low-velocity impacts (<4 km/s) resulted in smaller craters than sand targets. This is because energy dissipation by target grains disruption is not negligible compared to excavation energy. The trend of our results can not be explained by the classic πscaling by [4]. Quarter-space experiments suggest that cratering on coarse-grained targets would be divided into two stages: an early disruption stage and a latter excavation stage. We modified the scaling law based on the quarter-space observation, assuming that the momentum of an impactor transferred to a contacted target grain immediately, that is when a target grain size is larger than an impactor size, the effective velocity that controls the excavation field would be smaller. Using the new modified scaling law, we can estimate crater sizes on real-sized bodies.
Implications for mass loss rate: For example, on Itokawa (average surface grain size of 2 m) impactors smaller than 1 m might result in smaller craters than sand targets by 5 times at most and impactors smaller than 0.1 m rarely cause crater because they do not have enough energy to disrupt surface grains. In contrast, impactor larger than 1 m could form craters as large as craters on sand targets. When an impactor can fully disrupt a target grain, a crater is at least several times larger than a crater on rigid bodies such as rocks. Thus, the cratering mechanisms on large continuum asteroids and small rubble-pile asteroids might be very different. The mass loss on cratering could be assessed by the classic scaling law if the latter excavation mechanism is the same as cratering on sand targets. The rubble-pile asteroids can lose their mass easily compared to the same-sized rigid bodies due to larger craters. Resent observations of the small-main-belt asteroids suggest that smaller asteroids are depleted from the steady distribution decided by the catastrophic disruption with the slope of -3.5 (e.g., [5]). The high efficiency of mass loss among rubble-pile asteroids might be responsible for the lack of small asteroids.
[1] Pravec and Harris, Icarus 148, 12-20 (2000); Britt et al., Asteroids III, 485-500 (2002); Fujiwara et al., Science 312, 1330-1334 (2006) [2] Kobayashi and Tanaka, Icarus 206, 735-746 (2010) [3] Güttler et al., Icarus 220, 1040-1049 (2012); Holsapple and Housen, 46th LPSC, #2538 (2014) [4] Holsapple, Annu. Rev. EPS 21, 333-373 (1993) [5] Gladman et al., Icarus 202, 104-118 (2009)

Keywords: Asteroids, Impact experiments, Crater

Experimental study on propagation process of impact-induced seismic wave in quartz sand simulating asteroid regolith layer

*Kazuma Matsue[1], Masahiko Arakawa[1], Minami Yasui[1], Shota Takano[1], Sunao Hasegawa[2]

1.Graduate School of Science, Kobe University, 2.Institutes of Space and Astronautical Science, JAXA

Planetary explorations in the solar system have revealed that the asteroid surfaces were covered with the regolith layer made of boulders and granular materials. The surface morphologies of asteroids formed on the regolith layer were recently proposed to be modified due to the impact-induced seismic activity. Then, it is important for us to understand the physical mechanism of the impact-induced seismic vibration. Therefore, we carried out impact cratering experiments on quartz sand using a polycarbonate projectile to observe the seismic wave propagating through the sand (Matsue, (JPGU 2015)). Recently, we established a sabot-stopper method to launch various kinds of projectiles at a vertical type two stage light gas gun, then we performed the high-velocity impact experiments using a projectile made of different materials with the diameter of 2mm, and measured the impact-induced seismic wave. Based on the result of this study, we examined the attenuation rate of seismic wave in the quartz sand and the energy partition rate between the projectile kinetic energy and the kinetic energy of the seismic wave.
Impact cratering experiments were conducted by using a single stage vertical gun set at Kobe University and a two-stage vertical gun set at Japan Aerospace Exploration Agency (JAXA). The impact velocity was 0.2-6.9km/s using a polycarbonate projectile and 2,4,5km/s using a projectile made of different materials with a diameter 2mm: glass, aluminum, titanium, zirconia, stainless steel, copper and tungsten carbide. We used a quartz sand target with the particle diameter of 500μm and the bulk density of 1.48g/cm^3. The accelerometers were set on the target surface at different distances from the impact point. After each experiment, we measured the crater profile by using a laser profiler in order to acquire the crater shape quantitatively.
The crater shape formed by the polycarbonate projectile at different impact velocities showed the similarity, irrespective of the velocity, however the similarity was not followed by the results obtained by the projectile with different densities. Then, we found that the ratio of the crater depth to the diameter (d/D) was not constant and depended on the projectile density. On the other hand, the crater size is expressed by the π-scaling law. The impact induced seismic wave was classified into two categories according to the distance from the impact point: at the region far from the impact point, the seismic wave looks like a damped vibration wave, and at the region near the impact point, the seismic wave looks like a single pulse wave. It is noticeable that the peak value of the acceleration changes with the propagation distance: the maximum acceleration, g_{max}, has a power law relationship to the normalized distance x/R, where x is propagation distance and R is crater radius as follows, $g_{max}=10^{2.2\pm0.04}(x/R)^{-3.11\pm0.11}$. We calculated the impact-induced seismic efficiency factor, k; that is, the ratio of the impact-induced seismic energy to the kinetic energy of the projectile. The impact-induced seismic energy was assumed to be the kinetic energy of the quartz sand vibrating at the thin shell region with a width corresponding to one cycle of the seismic wave. As a result, the average of k was obtained to be $(8.1 \pm 5.0) \times 10^{-5}$ for the polycarbonate projectile impacts.

Keywords: crater, regolith layer, seismic shaking

Impact-driven flow-field: Hypervelocity material ejection from the interference zone

*Kosuke Kurosawa[1], Takaya Okamoto[1], Hidenori Genda[2]

1.Planetary Exploration Research Center, Chiba Institute of Technology, 2.Earth-Life Science Institute, Tokyo Institute of Technology

The scaling relationship of the excavated mass at a bin of ejection velocity has been widely explored to understand the effect of hypervelocity impacts on the material distribution on the planetary surface. The high-velocity component from the vicinity of the impact point, however, has not been investigated well probably because the mass of high-velocity component is likely to be a few orders of magnitude lower than the entire mass of impact ejecta. Nevertheless, such high-velocity component would mainly contribute to the material exchange between planets/satellites and the production of unique samples in strata on the Earth via aerodynamic heating during their flight in the atmosphere because there is a threshold velocity in such problems.
We meet three difficulties in the problems. Among them are (1) The point-source approximation cannot be applied because the excavation flow is expected to be driven by a shockwave generated during a projectile penetration, (2) a propagating shockwave interacts with a rarefaction wave from the free surface, leading to produce a complex flow field, which is referred to as the interference zone, and (3) the flow field cannot be solved analytically because of the non-linear nature of such flow field. Although Melosh (1984) approximately estimated the thickness of the interference zone and the ejection velocity under several assumptions, his model cannot be directly applied to the vicinity of the impact point within ~2-fold impactor foot print as pointed out by himself.
In this study, we analyzed such complex flow field using the iSALE shock physics code to obtain the highest velocity form the target surface. For simplicity, we calculated only vertical impacts. A cylindrical coordinate was employed. We used the Tillotson EOS for granite to treat the effects of thermal pressure due to irreversible shock heating on the change in the particle velocity. Although we assumed a spherical projectile with 10 km in diameter for reasons of expediency, the results can be converted to any size of projectile through appropriate scaling calculations because we did not include material strength and gravity in this calculation. The impact velocity was set to 12 km/s, which is a typical value of that to Mars and the Moon. Lagrangian tracer particles were inserted into each computational cell to obtain the change in the position, pressure, and energy as a function of its initial position. We analyzed the particles ejected within 3 seconds after the impact.
The particle motions are qualitatively consistent with the predictions by Melosh's model. It is important that the incidence angles of the shockwave and the rarefaction wave become nearly perpendicular in the interference zone. Thus, the accelerated materials by the shockwave suffer a further acceleration due to rarefaction wave in the upward direction. At this time, the stored internal energy due to the shock heating is converted to the kinetic energy of the upward motion. The highest ejection velocity determined by such acceleration is ~2-fold particle veloctity at the shocked state, which can be calculated using the Rankine-Hugoniot relations. Numerical calculations allow us to investigate the peak pressure at each position in the interference zone. The highest ejection velocity under the condition is ~5.5 km/s, which is about half of the impact velocity. The ejected mass at higher than 5 km/s is ~0.1 wt% of the projectile mass and they suffer the peak pressure of 40 GPa.
We are planning to do a series of numerical calculations to obtain the velocity-mass relation of the ejecta from the interference zone.

Keywords: Hypervelocity impacts, Impact ejecta, Martian meteorite

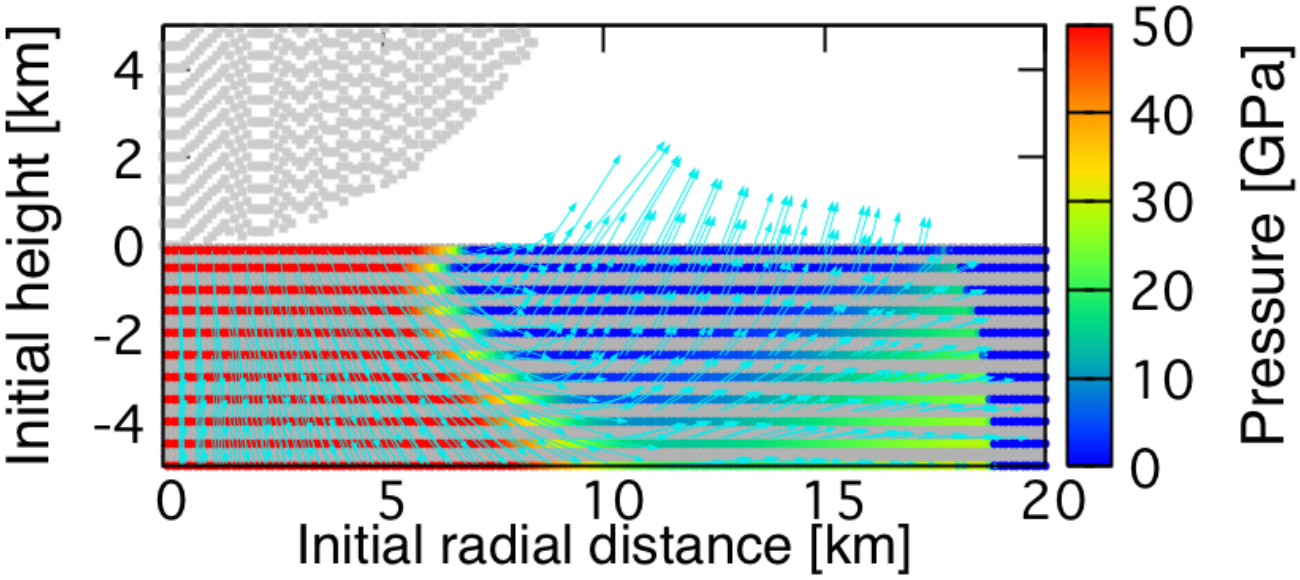

Water Partitioning into the Martian Mantle during Accretion of Mars

*Hiroaki Saito[1], Kiyoshi Kuramoto[1]

1.Department of Cosmosciences, Graduate School of Sciences, Hokkaido University

According to the latest analyses of Martian meteorites, the early Martian mantle was possibly wet with the H_2O concentration to be 780 ~ 2870 ppm (McCubbin et al., 2012). This estimate is equivalent to about 0.3~1 times the Earth ocean mass (~1.4×10^{21} kg) in the whole Martian mantle. Because of the lack of plate tectonics on Mars, water is likely to be partitioned to the interior during accretion of Mars. A planetary-scale magma ocean produced by the accretion energy and/or the blanket effect of the proto-atmosphere possibly absorbs a vast amount of water. However, it remains an open question how such a magma ocean could be formed on accreting Mars.
The precise Hf-W chronology suggests that the growth of Mars had been almost completed within the first several Myr after the formation of CAI (Dauphas and Pourmand, 2011: Tang and Dauphas, 2013), which is consistent with the theoretical estimate for the formation time of proto-planets. During such rapid accretion, a proto-Mars might gravitationally keep both degassed component and the solar nebula component as a proto-atmosphere. We call this atmosphere hybrid-type proto-atmosphere.
In this study, we analyze the thermal structure of hybrid-type proto-atmosphere by developing a 1D radiative-equilibrium model. Here we take into account the effect of the possible reduction of solar nebula pressure during accretion, taking the original nebula pressure at the Hill sphere to be 6.9×10^{-2} Pa (p_0) (Kusaka et al., 1970) and the minimum nebula pressure to be $10^{-12}\times p_0$. The accretion time is varied from 1 to 6 Myr so as to meet the chronological constraints. The building blocks of Mars is modeled by applying the two-component model (Wanke and Dreibus, 1988), which contains 35% of volatile-rich, oxidized CI chondritic material and 65% of volatile-poor, reduced E chondritic material. Impact degassing occurs for the planetesimal impacts with sufficiently high velocity as the growing Mars exceeds 0.1 times the final mass. Degassed volatile has a composition determined by the chemical equilibrium with molten silicate and metal produced by impact shock heating. Degassed component is assumed to occupy the lower atmosphere below the hydrogen-helium upper atmosphere continued to the solar nebula at the Hill radius.We solved the evolution of hybrid-type atmosphere with the growth of a proto-Mars. Independent of accretion time and nebula dissipation timescale, the proto-atmosphere is so massive and hot enough to produce the magma ocean during the last half stage of accretion. In the case without nebula dissipation, the surface pressure exceeds the solidus temperature 1500K of rock as the proto-Mars has grown larger than 0.3 times the final mass, and the surface pressure reaches ~2000bar at the end of accretion. On the other hand, in the case of lowered nebula pressure, the beginning of surface rock melting delays until the proto-Mars becomes larger than ~0.6 of its final mass due to the partial loss of degassed component to space, but the surface pressure still reaches ~ 800bar at the end of accretion. The amount of water partitioned into the magma is estimated to be ~9.6×10^{20} kg or larger. This value is equivalent to ~0.7 Earth ocean mass, which is basically consistent with the petrological evidence.

Keywords: Early Mars, Magma Ocean, Wet mantle

Diversity of atmospheric circulations of tidally locked gas giant planets -- dependence on the incident radiation strength

*Shin-ichi Takehiro[1], Yoshiyuki O. Takahashi[2], Kensuke Nakajima[3], Yoshi-Yuki Hayashi[2]

1.Research Institute for Mathematical Sciences, Kyoto University, 2.Department of Earth and Planetary Sciences, Kobe University, 3.Department of Earth and Planetary Sciences, Kyushu University

Thanks to recent development of observational instruments, the number of discovered exoplanets has been surprisingly increased. In particular, it is considered that there are many tidally locked gas giant planets, whose same hemispherical surfaces face to the central stars (hot Jupiter). General circulations of the surface atmospheres of such gas giants have been investigated using simplified and modified models for the Earth's atmospheric general circulation. One of the prominent characteristics of these simulations presented so far is a strong equatorial prograde jet (equatorial superrotation). However, the condition emerging a equatorial prograde jets is not well understood. Our purpose is to make clear the regimes of atmospheric general circulations of tidally locked gas giant planets through a series of numerical experiments using general circulation models where the parameters of the planetary atmospheres are widely varied, and understand diversity of atmospheric circulations of tidally locked gas giants. In this study, we investigate dependence on the incident radiation strength.
The atmospheric model used for numerical experiments is "DCPAM5" developed by GFD Dennou Club (http://www.gfd-dennou.org/library/dcpam/), which is a three-dimensional primitive model assuming hydrostatic balance in the radial direction. Dual band radiative transfer is adopted to express incident short wave radiation and outgoing long wave radiation. The incident radiation from the central star illuminates only the same hemisphere of the planet at all times. There is no heat flow through the bottom boundary. The parameters characterizing the planetary atmosphere in the model are based on those of the exoplanet HD209458b. Incident radiation strength is varied around the value of HD209458b. Time integrations are performed for various strength of incident radiation. When the incident radiation is as strong as that of the original HD209458b (10^6 W/m^2), strong equatorial prograde jet emerges which penetrates to about 1bar level. The equatorial jet is weakened and becomes shallow as the incident radiation is decreased. Finally, when the incident radiation is as weak as 10^3 W/m^2, equatorial zonal flows tend to retrograde and prograde high latitude jets become dominant. The newly found equatorial retrograde regime of tidally locked gas giants contrasts with that of equatorial prograde flow proposed so far.

Keywords: Hot Jupiter, Equatorial jets, Equatorial superrotation

A New Microphysical Model for Exoplanetary Clouds: Testing against the Observations of Terrestrial and Jovian Clouds.

*Kazumasa Ohno[1], Satoshi Okuzumi[1]

1.Department of Earth and Planetary Science, Graduate School of Science and Technology, Tokyo Institute of Technology

Recent transit surveys have shown that some close-in exoplanets have a featureless transmission spectrum. These planets are commonly thought to have high either an atmosphere with a high molecular weight or an optically thick dust cloud at a high altitude. A realistic exoplanetary cloud model is necessary to understand which interpretation is more likely for each exoplanets. Previous cloud models involve some free parameters whose relationship with the microphysics of the formation and growth of cloud particles is unclear. Furthermore, some models neglect the coalescence of dust cloud particles by assuming that micron-sized dust particles are unable to stick in an updraft.

We have been developed a new exoplanetary cloud model that involves the microphysics of condensation and coalescence (the Meeting of The Japanese Society for Planetary Sciences 2015). Our model produces the vertical distributions of the number and mass densities of cloud particles as a function of the atmospheric updraft velocity, the mixing ratio of the condensing gas at the cloud deck, and the number density of cloud condensation nuclei (CCN).

Here, we test the validity of our model by comparing with the observations of the clouds on the Earth and Jupiter. For terrestrial water clouds, we find that our model plausibly reproduces the cloud optical depth from satellite observations and vertical distributions of the mass and number densities of cloud particles from in situ observations. For Jovian ammonia clouds, our model simultaneously reproduces the particle effective radius, cloud optical depth, and cloud geometric thickness from far-infrared observations by assuming the updraft velocity of 1.2–2 m/s and CCN number density of ~5×10^{4} m^{-3}. The parameters values assumed for the Jovian clouds are consistent with the Galileo probe observation and with previous 2D simulations of moist convection in the Jovian atmosphere.

Keywords: exoplanet, cloud

A numerical experiment on occurrence condition of the runaway greenhouse state with a atmospheric general circulation model

*Masaki Ishiwatari[1], Satoshi Noda[2], Kensuke Nakajima[3], Yoshiyuki O. Takahashi[4], Shin-ichi Takehiro[5], Yoshi-Yuki Hayashi[4]

1.Faculty of Science, Hokkaido University, 2.Graduate School of Science, Kyoto University, 3.Department of Earth and Planetary Sciences,Flculty of Sciences,Kyushu University, 4.Graduate School of Science, Kobe University, 5.Research Institute for Mathematical Sciences, Kyoto University

Aiming for assessing the potential habitability of extrasolar terrestrial planets, the existence condition of liquid water on planetary surfaces has been discussed (e.g., Kasting et al., 1993). One of the main issues is the examination on the occurrence condition of the runaway greenhouse state. The runaway greenhouse state is defined as a state in which incident flux given to the atmosphere exceeds the radiation limit: the upper limit of outgoing longwave radiation (OLR) emitted from the top of the moist atmosphere on a planet with ocean (Nakajima et al., 1992). In the runaway greenhouse state, thermal equilibrium cannot be realized. Recent studies utilizing atmospheric general circulation models (AGCMs) discuss that atmospheric circulation and cloud albedo significantly affect the occurrence condition of the runaway greenhouse state (e.g., Leconte et al., 2013; Yang et al., 2013; Wolf and Toon, 2015). However, our speculation is that the runaway greenhouse state emerges when global mean absorbed solar radiation flux exceeds the maximum values of OLR. In order to confirm our speculation, we perform a numerical experiments with an AGCM. We examine the response of modeled atmospheric states to the increase of solar flux considering two spatial and temporal distributions: one for synchronously rotating planets with fixed dayside and nightside, and the other for an Earth-like, non-synchronously rotating planets with diurnal and seasonal changes. We use the AGCM developed by our research group, DCPAM (http://www.gfd-dennou.org/library/dcpam). Subgrid physical processes are parameterized with standard methods used in terrestrial Meteorology. The amount of cloud water is calculated with integrating a time dependent equation including generation, advection, turbulent diffusion, and extinction of cloud water. Extinction rate of cloud water is assumed to be proportional to the amount of cloud water, and extinction time is given as an external parameter. The entire surface is assumed to be a ``swamp ocean'' with zero heat capacity. The results of our experiment show that horizontal deviation of OLR decreases with increasing the value of solar constant regardless the radiation scheme (grey scheme or non-grey scheme), existence of clouds, and solar flux distribution. It seems that runaway greenhouse state appears when global mean absorbed solar radiation flux exceeds the maximum values of OLR. Our results suggest that the occurrence condition of the runaway greenhouse state is determined by a common mechanism, although the maximum value of OLR differs among runs with different conditions.

Keywords: runaway greenhouse state, exoplanet, radiation limit, atmospheric general circulation model, habitability

Two humidity regimes of stratosphere on a moist atmosphere

*Masanori Onishi[1], George HASHIMOTO[2], Kiyoshi Kuramoto[3], Yoshiyuki O. Takahashi[1], Masaki Ishiwatari[3], Yasuto TAKAHASHI[3], Yoshi-Yuki Hayashi[1]

1.Graduate School of Science, Kobe University, 2.Graduate School of Natural Science and Technology, Okayama University, 3.Graduate School of Science, Hokkaido University

An inner edge of habitable zone is characterized by runaway greenhouse limit and water loss limit. Kasting et al. (1993) and Kopparapu et al. (2013) estimated these limits by one-dimensional radiation transfer model. These studies assumed the isothermal atmosphere at 200K. This assumption, however, has a significant effect on the water loss limit because the limit is depend on the temperature of cold trap.Kasting et al. (2015) estimated the temperature profiles on planets with N_2, CO_2 and H_2O atmosphere by one-dimensional radiative-convective model. Their calculations suggest that the water loss limit can be estimated by an isothermal model, provided that one uses a stratospheric temperature of 150 K. Leconte et al. (2013) and Wolf & Toon (2015) calculated the temperature profiles by GCM and estimated that the stratosphere temperatures ware 140 ~ 150 K. These models used k-distribution method.Arking & Grossman (1972) estimated the temperature profiles of radiative equilibrium state by using an idealized semi-analytical non-grey radiative model. This study showed that in a non-grey atmosphere, the temperature increases with increasing mean opacity below a certain height and decreases with increasing mean opacity above that height. It also found that there is no lower limit to the temperature at the top of the atmosphere: it can approach zero arbitrarily closely as the width of the lines is decreased. This result implies that estimating temperature of upper part of atmosphere needs a high resolution calculation.In the temperature profiles estimated by previous studies, tropopause pressure is much lower than that in present-day Earth: 1000 ~ 1 Pa. On the other hand, these studies used the modified models from present Earth models. To estimate the temperature of higher tropopause, a radiative transfer model which calculates opacity of each wavelength accurately enough for estimating temperatures in lower pressure tropopause than that of Earth is required. We estimate the temperature by using such a one-dimensional, line-by-line radiative transfer model. The model atmosphere is assumed to consist of H_2O and N_2. The troposphere and stratosphere is assumed to be fully saturated and isothermal, respectively. The value of a heating rate in tropopause are calculated for various surface and tropopause temperatures. The wavenumber resolution of this model is 10^{-4} cm^{-1}, in 0 –3000 cm^{-1}; 10^{-2} cm^{-1}, 3000 –76576 cm^{-1}. The result shows the existence of two regime: one is dry regime, and the other is wet regime. In a dry regime, the tropopause temperature is about 120 K, that is independent of surface temperature. A wet regime, in which water vapor becomes a major constituent, appears when the surface temperature is higher than 345 K. The model atmosphere does not experience a water loss phase, instead skipping directly to a runaway greenhouse.

Keywords: moist atmosphere, radiative property, habitable zone, water loss limit

Search for Earth-like planets around late-M dwarf stars using the infrared Doppler

*Masashi Omiya[1,2], Takayuki Kotani[2,1], Motohide Tamura[3,2,1]

1.National Astronomical Observatory of Japan, 2.AstroBiology Center, 3.The University of Tokyo

We are proposing to conduct a strategic infrared Doppler survey for extrasolar Earth-like planets around M dwarf stars using a new astronomical infrared instrument (InfraRed Doppler instrument, IRD) for the Subaru telescope at Hawaii. For very precise radial velocity measurements in the infrared wavelength, IRD is composed of a stable astronomical high dispersion spectrograph and a laser-frequency comb as a precise wavelength calibrator covering the range of 0.97-1.75 micron. The main goals of the IRD survey are to achieve a radial velocity precision of 1m/s for late-M dwarfs and to search for Earth-like exoplanets around low-mass stars. Planetary systems around low-mass stars are attractive targets to detect extrasolar Earth-like planets in the habitable zone by the Doppler method because of relatively large signals caused by the planets and their close-in habitable zone. For the advantages of IRD and late-M dwarfs, we plan to perform a new unique large-scale planet search program to look for Earth-like planets by the Doppler method using the IRD and the Subaru telescope.
We have a plan to perform the first light of IRD in this summer and start the full-scale Doppler survey. In this survey, we would like to have 170 observing nights for 5 years from 2017 and observe ~100 carefully-selected late-M dwarfs. We performed a detailed survey simulation and target selection of suitable stars for the survey based on the theoretical simulation and real observation schedule. We will expect the discovery of more than 10 Earth-like planets in the habitable zone and more than 50 exoplanets for the survey period of 5 years. In this presentation, we report the current status of the construction and the observation plan and discuss expected detectable Earth-like planets and impacts on the exoplanet study in the Subaru/IRD survey.

Keywords: Earth-like planets, late-M dwarf stars, Infrared Doppler observation

Constraints on atmospheric pressure on early Mars inferred from nitrogen and argon isotopes

*Hiroyuki Kurokawa[1], Kosuke Kurosawa[2], Tomohiro Usui[3]

1.Earth-Life Science Institute, Tokyo Institute of Technology, 2.Planet. Explor. Res. Ctr., Chiba Institute of Technology, 3.Dept. of Earth & Planet. Sci., Tokyo Institute of Technology

Geomorphological evidence such as valley networks and deltas on Mars requires repeated episodes of liquid water runoff in the Noachian period. A dense atmosphere possibly caused water-ice being transported to the highlands. Fluvial terrains can be created by episodic melting events of ice under such conditions [1]. The dense atmosphere was lost from Mars, but the mechanism and timing are poorly constrained.
We constructed a one-box atmosphere-hydrosphere model with multiple species (CO_2, N_2, H_2O, and noble gases). We calculated the evolution of the volume and isotopic composition of the Martian atmosphere taking into consideration several processes, including impacts of asteroids and comets, atmospheric escape induced by solar radiation and wind, volcanic degassing, and a gas emission from interplanetary dust particles. A threshold for the atmospheric collapse (0.3 bar) was assumed following recent 3D global-circulation-model simulations [e.g., 2]. Comparing our results with nitrogen and argon isotopic compositions at 4.1 Ga recorded in Allan Hills (ALH) 84001 provided a lower limit of the atmospheric pressure on early Mars.
Since impacts mainly contribute to the evolution of atmosphere during the late accretion at 3.5-4.5 Gyr ago, the atmospheric pressure evolved stochastically for the first ~1 billion years. The atmospheric evolution depends on the volatile abundances in the impactors. In cases where relatively volatile-poor impactors were assumed, the impact erosion prevailed over the injection of volatiles and the atmospheric collapse occurs during this period.
Whereas the nitrogen ($^{15}N/^{14}N$) and argon ($^{38}Ar/^{36}Ar$) isotopic ratios kept unfractionated values before the collapse, they increased stochastically after the collapse. Impacts of asteroids and comets in a thinner atmosphere increased abundances of nitrogen and argon. It resulted in higher escape rates of these species and subsequently increased their isotope ratios. The cases of a moderately dense atmosphere (> 0.3 bar) at 4.1 Ga are consistent with unfractionated nitrogen and argon isotope ratios recorded in ALH 84001 [3]. This lower limit of the atmospheric pressure is valid regardless of the presence/absence of the Martian magnetic dynamo at 4.1 Ga because the atmospheric nitrogen was removed by photochemical escape driven by solar radiation.
The reported data on the trapped-nitrogen-isotope composition of ALH 84001 are highly scattered (~7 per mil to >200 per mil) in the literature. Identification of the actual nitrogen isotope ratio at 4.1 Ga would help to constrain the evolution of the Martian atmosphere.
Our results provided a lower limit of the atmospheric pressure at 4.1 Ga. If we combine our results with other constraints on the atmospheric pressure on early Mars [4], a moderately dense atmosphere (~0.1-1 bar) was suggested. We suggest that the moderately dense atmosphere was lost after 4.1 Ga by the impact erosion and the escape induced by solar radiation and wind.

[1] Wordswort, R. et al. (2013) Icarus, 222, 1-19. [2] Forget, F. et al. (2013) Icarus, 222, 81-99. [3] Mathew, K. J. & Marti, K. (2001) J. Geophys. Res., 106, E1, 1401-1422. [4] Kite, E. S. et al. (2014) Nature Geosci., 7, 335-339.

Keywords: Mars, Atmosphere, Isotopes

Shooting star formation in a laboratory experiment

*Hiroki Senshu[1], Kosuke Kurosawa[1], Takaya Okamoto[1]

1.Planetary Exploration Research Center, Chiba Institute of Technology

A shooting star is caused by an entry of a cosmic dust particle into the planetary atmosphere. The light from the shooting star composed of thermal emission and emission lines from the gas in from of the dust particle and the vapor from the dust particle. It means that the physical and chemical condition of the dust particle can be estimated from a photometric and/or spectroscopic observations. However a shooting star is a sporadic and un-controled event, and thus the relation between the physical and chemical condition and the resulting spectroscopic observation is estimated by empirical equations.
We are constructing a laboratory experimental system to simulate shooting stars by using a two-stage light gas gun at Planetary Exploration Research Center (PERC), Chiba Instiute of Technology, Japan. This gun shoots a projectile with size of 2 mm into a observational chamber filled with gas. The light from the projectile is observed by high-speed camera with 1 Mfps and its spectrum is taken by spectrometer simultaneously.
We carried out a series of experiments using the system with a variety of projectile composition. The specific spectra relating to the projectile component were confirmed as a function of the location from the projectile (during head-neck-tail structure). We will give the experimental results and discuss the chemical and physical status of shooting star.

Keywords: shooting star, impact, spectroscopy

Shock remanent magnetization measurement using the superconducting quantum interference device microscope

*Masahiko Sato[1], Kosuke Kurosawa[2], Masashi Ushioda[1], Sunao Hasegawa[3], Hirokuni Oda[1], Futoshi Takahashi[4], Jun Kawai[5]

1.National Institute of Advanced Industrial Science and Technology, 2.Chiba Institute of Technology, 3.Japan Aerospace Exploration Agency, 4.Kyushu University, 5.Kanazawa Institute of Technology

Knowledge of the evolution of magnetic field intensity is key to understanding the past evolution of planets. However, magnetic field paleointensity data of terrestrial planets such as Mars and Moon have been poorly obtained because of the lack of appropriate rock samples. To address the problem, we focus on shock remanent magnetization (SRM). There are many impact craters on surface of the terrestrial planets, and the magnetic field originated from the SRM of planetary crust can be measured by spacecraft magnetometer. The magnetic field paleointensity could be estimated using the magnetic field data observed over the impact craters.
In order to estimate the magnetic field paleointensity from the observed magnetic field data, it is crucial to know a structure of the SRM, while the structure remains unclear due to the difficulty in experimental techniques. In this study, to reveal the structure of SRM, we conducted SRM acquisition experiments and magnetic imaging of the SRM sample using the superconducting quantum interference device (SQUID) microscope.
Natural basalt samples with cylindrical form of 10 cm in diameter and 10 cm in length (FURNITURE STONE) were used as a target. Before the SRM acquisition experiments, the basalt samples were subjected to alternating field demagnetization at 80 mT. The two-stage light gas gun at the Institute of Space and Astronautical Science (ISAS) of Japan Aerospace and Exploration Agency (JAXA) was used for the SRM acquisition experiments. A magnetically shielded cylinder of 32 cm in diameter and 100 cm in length was set in a vacuum experimental chamber of the two-stage light gas gun. The magnetically shielded cylinder was constructed with three μ-metal layers, and the residual field in the cylinder was <0.3 μT. A solenoid coil of 26 cm in diameter was set in the magnetically shielded cylinder. The basalt sample was placed at the center of the solenoid coil. The applied field was set to be 0–100 μT, and direction of the applied field was parallel to the cylindrical axis of the basalt samples. An aluminum sphere of 2 mm in diameter was used as the projectile. A nylon slit sabot was used to accelerate the projectile. The impact velocity was ~7 km/s, and the impact angle was fixed at 90° from the horizontal.
Using the SQUID microscope at Geological Survey of Japan, National Institute of Advanced Industrial Science and Technology (AIST), magnetic imaging of the basalt samples were conducted after the SRM acquisition experiments. The basalt cylinder was placed on non-magnetic xyz-sample table. The distance between a surface of the basalt cylinder and the SQUID microscope was set to be ~1 cm, and a vertical component of magnetic field over the basalt sample was measured for 6 cm ×6 cm region. The sample imparted SRM in zero-field showed decrease in the magnetic field at center of the crater, corresponding to the increase in sample to sensor distance. On the other hand, the sample imparted SRM in a 100 μT field showed increase in the magnetic field at center of the crater. These results suggest that the basalt samples acquired remanent magnetization as the SRM. In this talk, we will discuss the structure of SRM based on the results of SQUID microscope measurements.

Keywords: Shock remanent magnetization, SQUID microscope

Collisional disruption of meter-sized boulders of the Moon

Kosuke Ando[1], *Tomokatsu Morota[1]

1.Graduate School of Environmental Studies, Nagoya University

The surface condition of planetary bodies reflects its geological evolution. Many boulders are observed on the surface of the Moon. It is thought that collisions of micro bodies disrupt boulders, and makes them fine. Recently, lunar explorations such as SELENE project and Lunar Reconnaissance Orbiter (LRO) obtained high-resolution images of the lunar surface. The high-resolution images allow us to perform statistic investigation of meter scale boulders on the lunar surface.
To reveal the time scale of boulder disruption on the Moon surface and to put constraints on dominant factors (for example, impacter frequency and boulder's strength) for boulder disruption, I performed size-frequency measurement of boulders (D >5 m) on ejecta of 19 small craters (D = 210–920 m), which exist on the floors of Copernicus crater (D = 92.5 km) and King crater (77.3 km). Also, the formation ages of the small craters were estimated from crater densities around the small craters.
The relationship between the boulder frequencies and the formation ages of the small craters indicates that the number densities of boulders decrease exponentially with time. The half-life period of boulder frequency in the King floor is estimated as 75 Myr, about 3 times longer than that in the Copernicus floor. A numerical model of boulder disruption reveals that the impactor frequency and boulder's strength have a significant influence on the survival time of boulders. The observed half-life period of boulders corresponds with a model for size-frequency distribution of impactors with a flatter slope.

Keywords: Moon, boulder, collisional disruption

Relation among the permittivity, density, and volume fraction of crack around craters formed by laboratory impact experiment

*Ken Ishiyama[1], Atsushi Kumamoto[1], Yasuhiko Takagi[2], Norihiro Nakamura[1], Sunao Hasegawa[3]

1.Tohoku University, 2.Aichi Toho University, 3.ISAS/JAXA

The lunar subsurface geological condition was investigated from the measurements of density of core sample [e.g., Carrier et al., 1991] and seismic velocity [e.g., Cooper et al., 1974] in Apollo site. These measurements suggests that the lunar subsurface density decreased with decreasing the depth, which is because there are more impact-induced cracks in the shallow media than in the deep media [e.g., Cooper et al., 1974]. Recently, in order to investigate lunar geological condition, the bulk permittivity of lunar subsurface layer was investigated based on the data from the Lunar Radar Sounder (LRS) onboard the SELENE (KAGUYA) spacecraft [Ishiyama et al., 2013]. Based on the empirical relation among the bulk permittivity, the bulk density, and the porosity, Ishiyama et al. [2013] suggested that the porosity of the lunar subsurface layer was ~19%. However, according to effective medium theory [e.g., Kärkkäinen et al., 2000], the direction of cracks in media can change the relation between the bulk permittivity and bulk density. In this study, we evaluate how the actual crack distribution around impact crater produced in the umpact experiment affect the bulk permittivity, and verify the validity of the estimation method of the porosity and bulk density from the permittivity measured in radar observations.

We performed the impact experiment by using the two-stage light-gas gun at JAXA. First, in order to produce two impact craters, the spherical stainless projectiles with a diameter of 0.32 cm, and mass of 0.133 g at the velocities of ~3.5 and ~5.5 km/s were impacted on two basalt targets with a size of 20 cm×20 cm×10 cm. Next, in order to investigate the influence of anisotropic cracks on permittivity, we drilled two core samples with a diameter of 2.5 cm and length of 8–10 cm along horizontal and perpendicular directions to its impacted surface from basalt target. Finally, we sliced the core sample, and produced sliced sample with a thickness of 3–4 mm. In order to identify the crack distribution on the surface of slice sample, the surface was polished.

In this study, we measured the bulk permittivity, bulk density, and volume fraction of crack of sliced sample. The permittivity of sliced sample was measured at 5 MHz, which is the same with center frequency of the LRS, by using the permittivity measurement system (TOYO Technica Corporation, Type-1260 impedance analyzer and Type-12962A interface). The density of the sliced sample was derived from the measurements of its mass and volume, and the volume fraction of crack of sliced sample was estimated from the ratio of the crack area to the total surface area of the sliced sample. The crack area was identified by applying an image processing to the picture of the surface of the sliced sample.

With the increase of radial distance from crater center, the volume fraction of crack decreased, and the density and permittivity increased. These parameters (i.e., permittivity, density, and volume fraction of crack) strongly depended on the characteristics of the crack distribution around impact crater. In addition, we could confirm difference between the permittivities of sliced samples including the cracks in different directions based on the comparison of slice samples from two core samples along horizontal and perpendicular directions to the surface impacted by the projectile at velocity of ~5.5 km/s. This difference of the permittivity could be explained by the effective medium theory [e.g., Kärkkäinen et al., 2000]. However, since the difference was enough small with respect to the deviation in the measurement of the permittivity of Apollo samples, we could conclude that the estimation method of the porosity and bulk density from the permittivity measured in radar observation was valid.

Experimental investigation on effect of particle size distribution and irregular shape on thermal conductivity of powdered materials

*Naoya Sakatani[1], Kazunori Ogawa[2], Masahiko Arakawa[2], Satoshi Tanaka[1]

1.Institute of Space and Astronautical Science, Japan Aerospace Exploration Agency, 2.Kobe University

Thermal conductivity of regolith on planetary bodies including the Moon and asteroids is one of the most important physical properties for calculating their surface temperature and thermal evolution. We have experimentally investigated the parameter dependences of the thermal conductivity of powdered materials under vacuum conditions mainly using glass beads as a model material. Together with these experimental results, we developed an integrative model for the thermal conductivity, which enable us to estimate the thermal conductivity of powdered materials from the parameter values. However, this model does not explicitly include the effects of particle size distribution and particle shape. Evaluation of their effects on the thermal conductivity is a critical issue to apply our thermal conductivity model to natural regolith on the planetary bodies.
In this study, we measured thermal conductivity of a lunar regolith simulant, JSC-1A, and samples with narrow particle size distributions prepared from JSC-1A by sieve. From these experimental results and our previous experiment data about the glass beads, we evaluated the effects of the wide particle size distribution and irregular particle shape on the thermal conductivity.
Particle sizes of JSC-1A is less than 1 mm, and volumetric median diameter and volumetric arithmetic mean diameter are about 100 μm and 40 μm, respectively. By sieving JSC-1A, we prepared four samples with particle sizes of 53-63 μm, 90-106 μm, 355-500 μm, and 710-1000 μm. We call the sample that is not sieved “JSC-O (Original)” and the samples that are sieved “JSC-S (Sieved)”. Their thermal conductivity was measured by the line heat source method. Degree of vacuum during the measurements was about 0.01 Pa, and ambient temperature was controlled from -25 to 60 ℃. Temperature dependence of the thermal conductivity for each sample was utilized to determine solid conductivity (contribution of the thermal conduction through contact points between the particles) and radiative conductivity (contribution of radiative heat transfer through void spaces between the particle surfaces). The particle size, density, and porosity of the measured samples are summarized in Table 1.
Figure 1 shows experimental results. Because the porosity values of the JSC-S were lower than that of JSC-O (42%) and were scattered from 47% to 66%, we corrected the conductivity to that at the porosity of 42% with using our thermal conductivity model, and these corrected data are also plotted. Moreover, the results for glass beads (porosity of 42%) are also shown.
(1) Effect of particle size distribution: Comparison of JSC-O and JSC-S.
We found that the solid conductivity of JSC-O is comparable with that of JSC-S of 90-106 μm. This particle size is comparable with the volumetric median size of JSC-O. That is to say, it implies that the solid conductivity of a powdered media with a given particle size distribution can be represented as that of a powdered sample with single particle size of the volumetric median. The radaitive conductivity of JSC-O was also comparable with JSC-S 90-106 μm. From these results, we can suggest that the particle size representative of the thermal property is the volumetric median particle diameter.
(2) Effect of particle shape: Comparison of JSC-S and glass beads
The solid conductivity values of JSC-S were comparable with or lower than those of glass beads with the same particle size of each JSC-S. These differences would reflect the difference of the particle shapes, and it is implied that irregular particles have lower solid conductivity than the

spherical particles. On the other hand, we found that the radiative conductivity values of JSC-S and glass beads were comparable. Therefore, we can conclude that the effect of the particle shape on the radiative heat transfer is small, and the radiative conductivity can be modeled with approximation by spherical particles.

Keywords: Regolith, Thermal conductivity

Table 1: Sample list

Sample	Particle size	Density	Porosity
JSC-O	< 1000 μm median 100 μm	1690 kg/m^3	42%
JSC-S	710-1000 μm	980 kg/m^3	66%
	355-500 μm	1110 kg/m^3	62%
	90-106 μm	1460 kg/m^3	50%
	53-63 μm	1540 kg/m^3	47%

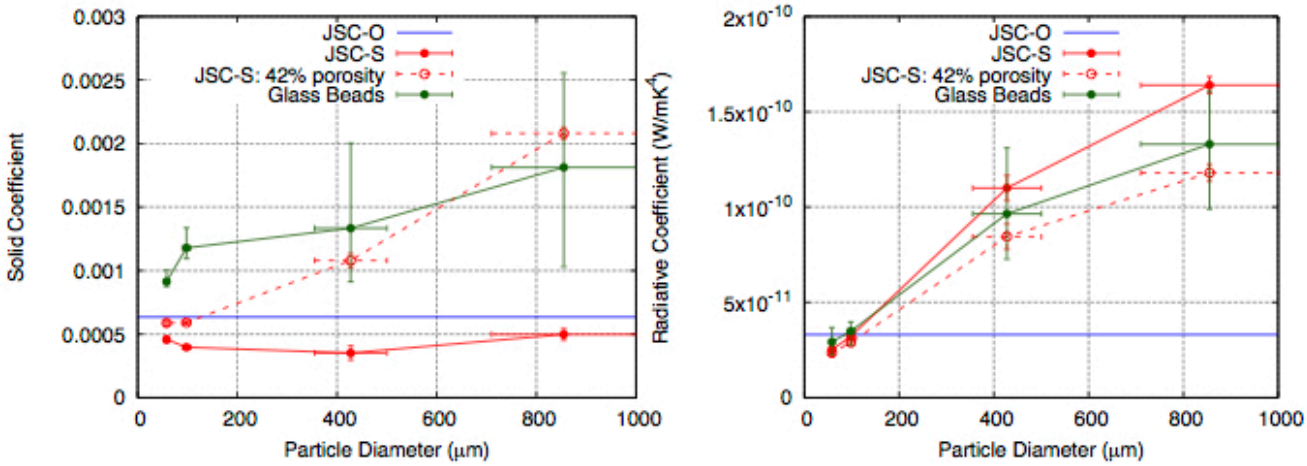

Figure 1: Solid (left) and radiative (right) coefficient of JSC-O (blue), JSC-S (red), and glass beads (green). Dashed red points represent each coefficient that is corrected to porosity of 42%.

Initial operation of Hayabusa2 laser altimeter (LIDAR)

*Hirotomo Noda[1], Takahide Mizuno[2], Noriyuki Namiki[1], Hiroki Senshu[3], Hiroo Kunimori[4], Naoko Ogawa[2], Hiroshi Takeuchi[2], Makoto Shizugami[1]

1.National Astronomical Observatory of Japan, 2.Japan Aerospace Exploration Agency, 3.Chiba Institute of Technology, 4.National Institute of Information and Communications Technology

The Hayabusa2 asteroid explorer was launched on December 3,2014. The spacecraft orbited around the Sun for a year, and after an Earth Gravity Assist operation, the spacecraft was inserted into a transfer orbit to the target asteroid 162173 Ryugu for the arrival at 2018. The first checkout of a laser altimeter called LIDAR onboard Hayabusa2 was done on January 23, 2015, and a rehearsal operation for the coming laser link experiment was done on August 27, 2015, and the laser link experiments had been done between October and December 2015. In this paper, we will discuss the following three issues of the LIDAR based on the result of the initial operation.i) Estimation of the boresight direction of the receiving telescope: We conducted an experiment in which laser pulses were transmitted toward the LIDAR from ground-based satellite laser ranging stations and the LIDAR bounced the laser toward the Earth. We call the experiment as laser link experiment. In this experiment, we set the observational mode as “optical transponder” mode. As the boresight direction was not determined well at first, the attitude of the spacecraft was scanned spirally outward from a center with 1 mrad separation, and the direction of the boresight of the receiving telescope was estimated when the LIDAR detected the laser pulses from the ground. Based on results of three days experiment, we found out that the boresight direction was closer with 0.2 degrees to the -Z axis of the spacecraft compared with what was measured before the launch with alignment cubes. However, the estimated boresight directions differs about 1 mrad for each day. So far we do not have any good reasons for that. Therefore, we concluded that the boresight was determined with the ambiguity of 1 mrad, and it must be updated after arriving at the target asteroid by detecting notable topographic features. The alignment between the transmitting and the receiving telescope has not been confirmed yet, because we have not detected the downlink laser pulses from the LIDAR on the ground station.ii) Confirmation of the ranging function: In the normal ranging, a gate is set just after the laser is transmitted to inhibit the detection of the laser. As a checkout of the instrument, however, we did not set the gate so that the scattered stray light can be detected to make the ranging circuit operated. We call this operation “non-gate ranging”. During the initial checkout, we conducted the non-gate ranging for three times, on January 23,August 27, and December 16. We confirmed that the ranging circuit worked without any problem on each day. The value of the pseudo range (the time between transmission and reception of the laser) did not show any change for each day. The averaged laser power was also confirmed normal, taking into account the deviation from the averaged value. The reception power changed in accordance with the transmission energy. Considering all these evidences, we concluded that the ranging function was normal.iii) Evaluation of the reception noise level: In both ranging mode and optical transponder mode, we observed such phenomenon that the detection flags became ON thought the reception power showed zero, and that the frequency of this phenomenon increased as the smaller threshold level of the reception was set. Assuming that this was because of the noise from the AD converter, we conducted a test operation on August 27 to clarify the boundary in which the frequency increased. As a result, we found that the threshold level at which noise increased as between 12 mV and 14 mV. In the ranging mode, the recommended threshold level is 27 mV or 45 mV, therefore practically the influence of the noises will be insignificant. However, in the “dust counting mode” which aims to detect the levitation dust near the asteroid, the threshold will be set comparable or lower than this value, because the

detection level estimated from the dust flux is expected to be low.

Keywords: Hayabusa2, asteroid, laser altimeter

JUICE/GALA-J (1) : The Ganymede Laser Altimeter (GALA) for the JUICE mission - Introduction, current status, and role of the Japan team

*Keigo Enya[1], Noriyuki Namiki[2], Masanori Kobayashi[3], Jun Kimura[4], Hiroshi Araki[2], Hirotomo Noda[2], Shoko Oshigami[2], Shingo Kashima[2], Ko Ishibashi[3], Shingo Kobayashi[5], Masanobu Ozaki[1], Takahide Mizuno[1], Shin Utsunomiya[1], Yoshifumi Saito[1], Kazuyuki Touhara[1], Shunichi Kamata[5], Koji Matsumoto[2], Kiyoshi Kuramoto[5], Sho Sasaki[6], Satoru Iwamura[7], Teruhito Iida[8], Yoshiaki Matsumoto[8], Masanori Fujii[9], Naofumi Fujishiro[10], Tomoyasu Yamamuro[11], Kay Lingenauber[12], Thomas Behnke[12], Juergen Oberst[12], Judit Jaenchen[12], Horst-Georg Loetzke[12], Harald Michaelis[12], Hauke Hussmann[12]

1.JAXA/ISAS, 2.NAOJ, 3.CIT, 4.Earth-Life Science Institute, Tokyo Institute of Technology, 5.Hokkaido University, 6.Osaka University, 7.MRJ, 8.PLANET, 9.FAM Science, 10.Astro-Opt, 11.OptCraft, 12.DLR

We present an introduction, current status, and especially role of the Japan team for the Ganymede Laser Altimeter (GALA) for the Jupiter Icy Moon Explorer (JUICE) mission. JUICE is a mission of ESA to be launched in 2022, and GALA is one of the payloads of JUICE.
Major objectives of GALA are to provide topographic data of Ganymede, the largest satellite of Jupiter, and to measure its tidal amplitudes. The latter is crucially important to detect and to characterize an underground ocean on Ganymede. Furthermore, GALA support geological studies, e.g., identification of characterization of tectonic and cryo-volcanic regions, impact basins, and craters. GALA also provides information on surface roughness and the albedo.
For the laser altimetry, GALA emits and receives laser pulses at about 500 km altitude above Ganymede. Wavelength, energy, and nominal repetition frequency of the laser pulse are 1064 nm, 17 mJ, and 30 Hz, respectively. Reflected beam from the Ganymede surface is received by the receiver telescope with 25 cm diameter aperture, re-focused by the BEO including a narrow band-pass filter, and then detected by the APD detector.
Development of GALA is carried out in international collaboration from Germany, Japan, Switzerland, and Spain. GALA-Japan will develop the Backend Optics (BEO), the Focal Plane assembly (FPA) including an avalanche photo-diode (APD) detector, and the Analog Electronics module (AEM) in the receiver chain. It should be noted that responsibility of development of the receiver telescope has been moved from Japan to Germany. Based on the heritage of studies for the telescope, GALA-Japan will contribute to the receiver telescope development through the German team.

Keywords: JUICE, GALA, Jupiter, Icy moon, Ganymede, Laser altimeter

Orbital and tidal evolution of Enceladus

*Ayano Nakajima[1], Shigeru Ida[1], Jun Kimura[2]

1.Department of Earth and Planetary Sciences, Tokyo Institute of Technology, 2.Earth-Life Science Institute, Tokyo Institute of Technology

Among Saturn's mid-sized moons, only Enceladus is thermally active, which has been a big puzzle. We have performed numerical simulations of tidal orbital evolution of the Saturn's mid-sized moons and evaluated tidal heating in Enceladus.
The current heat flux of Enceladus was estimated as ~16 GW by Cassini's observation (Howett et al. 2011). If the time-averaged dissipation factor Q of Saturn is anticipated as ~18000, the heat production is estimated to be 1.1 GW (Meyer & Wisdom 2011), which is much smaller than the observed value. Recently, a smaller value of Q_{Saturn} (~1680) was suggested by astrometric data analysis (Lainey et al. 2010). If Q_{Saturn}=1680, the mid-sized satellite may have formed from the ring (Charnoz et al. 2011). In this model, Enceladus must be formed earlier than Tethys and their orbits must closely approach each other in the course of tidal orbital evolution.
Through numerical orbital integration taking into account tidal interactions, we found that Enceladus is captured at a mean-motion resonance with Tethys. Because Tethys is more massive and accordingly its orbital evolution is faster, Enceladus' semi-major axis is pushed by Tethys and its eccentricity is secularly increased until its orbit starts crossing with Tethys' orbit. Eventually, Enceladus is scattered inward and Enceladus and Tethys establish the current orbital order. After the inward scattering, Enceladus becomes isolated from Tethys and its large eccentricity is damped by tidal dissipation inside Enceladus. The heat generation may be large enough to account for the current heat flux. Because this process occurs only for Enceladus, it can explain why only Enceladus is thermally active.

Keywords: Enceladus, tidal heating, orbital evolution, mean motion resonance

Interior thermal state of Enceladus: an inference from the relaxation state of its icy shell

*Shunichi Kamata[1], Francis Nimmo[2]

1.Creative Research Institution, Hokkaido University, 2.UC Santa Cruz

The South Polar Terrain of the icy Saturnian satellite, Enceladus, is one of the most geologically active regions among icy worlds. The origin of the anomalously large amount of heat observed over this region by the Cassini spacecraft is still unclear. To understand the heat budget of Enceladus, the interior thermal state should be investigated. This study attempts to constrain the thermal structure of Enceladus by comparing two timescales: those for viscous relaxation and melting. The subsurface ocean underneath the South Polar Terrain is thicker than other areas; the crust is thin in this region. Such “topography” at the base of the shell should viscously relax over time, and its timescale depends on the temperature of the deep part of the shell. If the shell is hot and has a low viscosity, the relaxation timescale should be short; a regionally thickened subsurface ocean cannot be maintained.On the other hand, if the laterally flowing portion of the shell melts, then a regionally thickened subsurface ocean can be maintained. In this study, we conduct numerical calculations of viscoelastic deformation under a wide variety of parameter conditions and compare timescales of viscoelastic relaxation and melting of the shell. Our results indicate that the former timescale is much shorter than the latter if we consider conventional values for radiogenic heating (0.3 GW [Roberts & Nimmo, 2008]) and tidal heating (1.1 GW [Meyer & Wisdom, 2007]). Our results also indicate that >10 GW, about one order of magnitude larger than the conventional value, is necessary to make those timescales comparable. This result suggests that the current Enceladus is unlikely to be in a steady-state; previous episodic heat production may contribute significantly to the current thermal state of Enceladus.

Keywords: Enceladus, Icy satellite, Viscoelastic

Numerical experiments on mantle convection of super-Earths with variable thermal conductivity and adiabatic compression

*Masanori Kameyama[1], Mayumi Yamamoto[1]

1.Geodynamics Research Center, Ehime University

We conduct a series of numerical experiments of thermal convection of highly compressible fluid in a two-dimensional rectangular box, in order to elucidate the mantle convection on super-Earths. The thermal conductivity and viscosity are assumed to exponentially depend on depth and temperature, respectively, while the variations in thermodynamic properties (thermal expansivity and reference density) with depth are taken to be relevant for the super-Earths with 10 times the Earth's. Our experiments showed the change in convecting flow patterns depending on the depth-dependence in thermal conductivity and the temperature-dependence in viscosity. This is largely due to the change in the thermal state in the convecting mantle, whose interplay with the adiabatic temperature change in turn reduces the activity of hot plumes from the base of the mantle. In particular, for the cases with strong interplay, we found that a "deep stratosphere" of stable thermal stratification can form at the base of the mantle where the fluid motion is insignificant. We also found that the presence of "deep stratosphere" not reduces but enhances the overall heat transport through the mantle, although it weakens the vigor of mantle convection. Our finding may further imply that the absence of intrinsic magnetic fields on massive terrestrial planets is not a corollary of the lack of plate tectonics on their surfaces.

Keywords: super-Earths, mantle convection, adiabatic (de)compression

High dimensional coupled spin model for polarity reversals

*Ariyoshi Kunitomo[1], Akika Nakamichi[2], Tetsuya Hara[1]

1.Kyoto Sangyo University, 2.Koyama Astronomical Observatory, Kyoto Sangyo University

Recently, the macro spin model has been suggested for polarity reversal (Nakamichi et al. 2012, Mori et al. 2013). This is the idea that geomagnetism is described by interaction with many local dynamo elements (called macro-spins). This model can reproduce many features of geomagnetism and the solar magnetism; power spectrum, average time of polarity flipping, randomness and periodicity of polarity reversals.We study this model to become higher dimensional model. In this result, our model becomes possible for many things which are not treated in previous study, for example reproduce migration of the North (or South) Magnetic Pole, comparison with observed data of magnetic field distributions expressed in two directions.In addition, we investigate some distribution function that the pole migration followed and make a comparison with previous study, e.g. Lévy distribution (Carbone et al., 2006) and log-normal distribution (Ryan & Sarson, 2007).

Keywords: geomagnetism, solar magnetism, coupled-spin

